

Biomolecules and Biomedicine ISSN: 2831-0896 (Print) | ISSN: 2831-090X (Online)

Journal Impact Factor® (2024): 2.2

CiteScore® (2024): 5.2

www.biomolbiomed.com | blog.bjbms.org

The BiomolBiomed publishes an "Advanced Online" manuscript format as a free service to authors in order to expedite the dissemination of scientific findings to the research community as soon as possible after acceptance following peer review and corresponding modification (where appropriate). An "Advanced Online" manuscript is published online prior to copyediting, formatting for publication and author proofreading, but is nonetheless fully citable through its Digital Object Identifier (doi®). Nevertheless, this "Advanced Online" version is NOT the final version of the manuscript. When the final version of this paper is published within a definitive issue of the journal with copyediting, full pagination, etc., the new final version will be accessible through the same doi and this "Advanced Online" version of the paper will disappear.

RESEARCH ARTICLE

Zhou et al: Zbp1 necroptosis and inflammation in ALI

Mitochondrial dysfunction triggers Zbp1-mediated necroptosis and inflammation in acute lung injury

Mi Zhou¹, Yuehan Li¹, Yinying Ren¹, Yan Li¹, JinYing Xiang¹, Fang Deng¹, Gang Geng¹, Jian Luo¹, Jinyue Yu^{2,3}, Zhou Fu¹, Fengxia Ding^{1*}, Bo Liu^{4*}

¹Department of Pediatric Respiratory Medicine; National Clinical Research Center for Child Health and Disorders; Ministry of Education Key Laboratory of Child Development and Disorders; China International Science and Technology Cooperation Base of Child Development and Critical Disorders; Chongqing Engineering Research Center of Stem Cell Therapy, Children's Hospital of Chongqing Medical University, Chongqing, China;

²Bristol Medical School, University of Bristol, Bristol, UK;

³Great Ormond Street Institute of Child Health, University College London, London, UK;

⁴Department of Pediatric Cardiothoracic Surgery; National Clinical Research Center for Child Health and Disorders; Ministry of Education Key Laboratory of Child Development and Disorders; China International Science and Technology Cooperation Base of Child Development and Critical Disorders; Chongqing Engineering Research Center of Stem Cell Therapy, Children's Hospital of Chongqing Medical University, Chongqing, China.

*Correspondence to Fengxia Ding: <u>482613@hospital.cqmu.edu.cn</u> and Bo Liu: <u>lbcqmu@126.com</u>.

DOI: https://doi.org/10.17305/bb.2025.13046

ABSTRACT

Acute lung injury (ALI) is driven by dysregulated inflammation, but how mitochondrial damage engages necroptosis in alveolar macrophages remains unclear. We aimed to define the mechanistic link between mitochondrial impairment and Zinc finger protein 1 (Zbp1)-mediated necroptosis in the murine alveolar macrophage-like cell line (MH-S). MH-S cells were stimulated with lipopolysaccharide (LPS) and profiled by RNA sequencing; necroptotic death was quantified by Calcein-AM/propidium iodide (PI) staining and lactate dehydrogenase (LDH) release, Zbp1 localization was examined by immunofluorescence microscopy, and Zbp1, receptorinteracting protein kinase 3 (RIPK3)/phospho-RIPK3 (p-RIPK3) and mixed lineage kinase domain-like protein (MLKL)/phospho-MLKL (p-MLKL) were measured by Western blotting. Mitochondrial status was assessed by mitochondrial reactive oxygen species (mtROS), mitochondrial membrane potential (ΔΨm; JC-1), mitochondrial permeability transition pore (MPTP) opening, adenosine triphosphate (ATP) content, and the markers ATP synthase F1 subunit alpha (ATP5a1), mitochondrial transcription factor A (TFAM), and translocase of outer mitochondrial membrane 20 (TOMM20); inflammatory responses were quantified by flow cytometry and qPCR. The mitochondria-targeted antioxidant Mito-TEMPO was used to interrogate the role of oxidative stress. LPS markedly increased Zbp1 transcription, coincident with upregulation of pro-inflammatory genes and activation of necroptosis; mitochondrial damage and elevated mtROS were critical upstream events for Zbp1 induction, driving RIPK3 and MLKL phosphorylation, necroptosis, and cytokine release. Mito-TEMPO restored mitochondrial function, lowered mtROS, downregulated Zbp1 and its necroptotic effectors (p-RIPK3, p-MLKL), and significantly reduced both necroptotic injury and inflammatory output. Collectively, mitochondrial dysfunction driven mtROS initiates the Zbp1/RIPK3/MLKL necroptotic axis in alveolar macrophages, thereby amplifying pulmonary inflammation in ALI; targeting mtROS may mitigate necroptosis and protect against lung injury.

Keywords: Acute lung injury, alveolar macrophages, mitochondria, Zbp1.

INTRODUCTION

Acute lung injury (ALI) represents a critical clinical syndrome marked by extensive damage to the alveolar epithelium and heightened, poorly controlled inflammation, which collectively contribute to its high rates of morbidity and mortality worldwide^[1-3]. Although its development involves multiple pathological factors, a central hallmark of ALI is immune dysregulation that drives the progression of inflammatory injury within the lungs^[4]. Alveolar macrophages (AMs), as sentinel immune cells residing in the pulmonary microenvironment, are essential in detecting tissue damage and coordinating immune responses^[5]. Nevertheless, the precise mechanisms through which their dysfunction leads to exaggerated inflammation in ALI remain insufficiently characterized.

Mitochondria, beyond their conventional role in energy metabolism, act as critical hubs for maintaining cellular integrity, regulating redox balance, and modulating programmed cell death^[6,7]. In recent years, mitochondrial derangement has emerged as a pivotal contributor to inflammation and tissue injury across various disease contexts, including ALI^[8]. Of particular interest are mitochondrial quality control (MQC) systems and cell death pathways, which are tightly intertwined and fundamental to maintaining lung homeostasis^[9-12]. Disruption of MQC, alterations in mitochondrial dynamics, and compromised membrane integrity can result in oxidative stress and the release of damage-associated molecular patterns (DAMPs), thereby enhancing inflammatory signaling cascades^[13]. Moreover, mitochondrial stress has been implicated in activating necroptosis, a form of regulated necrosis characterized by loss of membrane integrity and pro-inflammatory cellular disintegration^[14].

Necroptosis is mediated through a well-defined signaling cascade involving receptor-interacting protein kinases RIPK1 and RIPK3, which activate mixed lineage kinase domain-like protein (MLKL) through phosphorylation. This results in MLKL oligomerization and disruption of the plasma membrane^[15]. Unlike apoptosis, necroptosis proceeds independently of caspases and provokes robust inflammation, thus acting as a key link between cell death and immune activation in various inflammatory conditions^[16]. Recent discoveries have identified Zinc finger protein 1 (Zbp1), a cytosolic RHIM-containing sensor, as an upstream activator of RIPK3-dependent necroptosis^[17]. While Zbp1 has been implicated in antiviral responses and

chronic inflammation, its role in ALI, especially in the context of mitochondrial damage, remains poorly understood.

Given the pivotal role of alveolar macrophages in regulating pulmonary inflammation during ALI, it is imperative to investigate how their mitochondrial integrity influences Zbp1-driven necroptotic signaling. This study aims to dissect the crosstalk between mitochondrial impairment in AMs and the initiation of Zbp1-mediated necroptosis in the pathogenesis of ALI. Clarifying these molecular interactions may reveal novel mechanistic insights and offer potential therapeutic strategies to ameliorate inflammatory lung injury.

MATERIALS AND METHODS

Transcriptome profiling of MH-S cells treated with LPS

The murine alveolar macrophage-like MH-S cell line (5 × 10⁶ cells/group) was cultured under both baseline and LPS-stimulated conditions. Total RNA was extracted using 1 mL of TRIzol reagent (TIANGEN, China). The extracted RNA was then used for library preparation and sequencing, which were carried out by Shanghai Biotechnology Corporation. Complementary DNA (cDNA) libraries were constructed following the TruSeq® RNA Sample Preparation guidelines, and final libraries were generated through PCR-based amplification.

After purification, library quality and concentration were evaluated. Sequencing was conducted using the Illumina HiSeq 2500 platform (Illumina, USA). Raw reads were processed to obtain transcriptomic profiles. Differentially expressed genes (DEGs) were identified using the edgeR statistical package, with significance criteria set at |log₂ fold change| ≥ 1 and adjusted *p*-value < 0.05. To explore the biological implications of LPS exposure in MH-S cells, Gene Ontology (GO) and Kyoto Encyclopedia of Genes and Genomes (KEGG) pathway analyses were conducted using the DAVID bioinformatics resource (version 2021; http://david.ncifcrf.gov). The STRING database(version 12.0; https://cn.string-db.org/) was used to identify potential interacting partners of Zbp1, and a subsequent Reactome pathway enrichment analysis was then performed to elucidate its functional context within biological pathways.

Cell culture and treatments

MH-S murine alveolar macrophages (ATCC CRL-2019) were maintained in RPMI-1640 medium (Gibco, USA) enriched with 10% fetal bovine serum (FBS; VivaCell, China) under standard incubation conditions (37 °C, 5% CO₂). To induce an inflammatory response, cells were exposed to lipopolysaccharide (LPS; Solarbio, China) at concentrations of 0.5 μg/mL or 1 μg/mL for a duration of 12 hours. Post-stimulation, cells were collected for further experimental procedures. To evaluate the involvement of mitochondrial reactive oxygen species (mtROS), Mito-TEMPO (MT; MedChemExpress, China) was used at 100 μM. MT was added 30 minutes before LPS treatment to suppress the accumulation of mtROS.

Lactate dehydrogenase (LDH) release detection

MH-S cells were cultured in 96-well plates and treated with lipopolysaccharide (LPS, Solarbio, China) at concentrations of 0.5 μg/mL or 1 μg/mL for 12 hours. After stimulation, the supernatant was harvested to assess lactate dehydrogenase (LDH) release using a commercial LDH cytotoxicity detection kit (Beyotime, China) according to the supplier's instructions. Absorbance at 450 nm was recorded using a BioTek multi-mode microplate reader (USA).

Cellular immunofluorescence

MH-S cells were first stained with MitoTracker Red at 37 °C for 30 minutes in the absence of light. Following incubation, cells were fixed using 4% paraformaldehyde, permeabilized with 0.1% Triton X-100 (Beyotime, China) for 20 minutes, and subsequently blocked with 5% bovine serum albumin (BSA; Solarbio, China) at ambient temperature for 30 minutes. Cells were then incubated overnight at 4 °C with a rabbit-derived primary antibody against murine Zbp1 (cat.#:13285-1-AP, Proteintech, China; dilution 1:100). After washing, they were treated with FITC-labeled goat anti-rabbit IgG secondary antibody (cat.#:A0562, Beyotime, China; dilution 1:250) for 1 hour in the dark. Nuclear staining was performed using DAPI (cat.#:C1006, Beyotime, China; dilution 1:500) for 10 minutes at room temperature. Confocal images were acquired using a laser scanning microscope (Nikon, Japan).

Mitochondrial reactive oxygen species (mtROS) detection

To evaluate mitochondrial reactive oxygen species (mtROS) production in MH-S cells, the fluorescent probe MitoSOX Red (5 μ M) was applied. The cells were incubated with the dye at 37 °C for 30 minutes under light-protected conditions, then rinsed three times with PBS. Imaging was performed using a laser-scanning confocal microscope (Nikon, Japan), and fluorescence intensity was quantitatively analyzed by flow cytometry (BD Biosciences, USA).

Mitochondrial membrane potential (ΔΨm) assessment

Mitochondrial membrane potential (ΔΨm) was assessed using the JC-1 assay kit (Beyotime, China). MH-S cells were first rinsed with phosphate-buffered saline (PBS), then incubated in JC-1 working solution at 37 °C for 30 minutes under dark conditions. Following incubation, unbound dye was eliminated by washing with pre-chilled staining buffer. The fluorescence signal ratio (aggregated red vs. monomeric green) was subsequently analyzed via fluorescence microscopy (Nikon, Japan) and quantified using a flow cytometer (BD Biosciences, USA).

Mitochondrial permeability transition pore (MPTP) opening detection

The mitochondrial permeability transition pore (MPTP) status was evaluated utilizing a commercial assay kit (Beyotime, China). MH-S cells were treated with Calcein-AM in combination with cobalt chloride to quench cytosolic fluorescence, followed by a 30-minute incubation at 37 °C in the absence of light. After thorough washing, cellular fluorescence was observed under a fluorescence microscope (Nikon, Japan) and quantitatively measured by flow cytometry (BD Biosciences, USA).

Adenosine triphosphate (ATP) measurement

Cellular ATP levels were quantified using an enhanced luminescence-based ATP detection kit (Beyotime, China). After treatment with the lysis buffer provided in the kit, cell lysates were centrifuged to obtain the supernatant. A standard curve was generated using serial dilutions of ATP standards, and the detection reagent was prepared as instructed. Luminescence signals were recorded with a multifunctional microplate reader (BioTek, USA). Protein content was assessed by measuring absorbance at 280 nm, and ATP levels were normalized to total protein concentration.

Flow cytometry

MH-S cells were immunolabeled using anti-CD86 allophycocyanin (PE) and anti-CD206 phycoerythrin (APC) antibodies (eBioscience, USA) to characterize their surface markers. The cells were incubated with these antibodies at 4 °C for 30 minutes in the dark, followed by washing with PBS. Subsequent analysis was conducted on a FACS Canto II flow cytometer (BD Biosciences, USA), with marker levels quantified by fluorescence intensity.

To evaluate necroptosis, the Calcein/PI Cell Viability/Cytotoxicity Assay Kit (Beyotime, China) was utilized. After washing twice with chilled PBS, cells were resuspended in 1× Binding Buffer and incubated with Calcein-AM and propidium iodide (PI) dyes for 30 minutes at room temperature in the dark. Immediately afterward, stained cells underwent flow cytometric analysis. To exclude the involvement of alternative cell death pathways, Zbp1-knockdown MH-S cells were co-treated for 4 hours with the pyroptosis inducer Nigericin (5 μg/mL; TargetMol, China), the apoptosis inducer Staurosporine (1 μM; TargetMol, China), or the ferroptosis inducer RSL3 (10 μM; TargetMol, China). FlowJo software (Version 10.8.1) was used for data processing.

Quantitative real-time PCR (qRT-PCR)

Total RNA was isolated following the manufacturer's instructions using an RNA extraction kit (BioFLUX, China). Equivalent amounts of RNA were then reverse transcribed into complementary DNA (cDNA) with a reverse transcription kit (Accurate Biology, China). Quantitative real-time PCR (qRT-PCR) was conducted using SYBR qRT-PCR Premix (Accurate Biology, China) according to the provided protocol. For analysis of mitochondrial RNA, mitochondria were first purified from MH-S cells employing a mitochondrial isolation kit (Beyotime, China), after which RNA was extracted to assess mitochondrial Zbp1 transcript levels. β -actin or 18s rRNA were used as reference genes for normalization. Relative expression was calculated using the $2^-\Delta\Delta$ Ct approach. Primer sequences used in this study are listed in Table S1.

The isolated mitochondrial fraction was diluted 100-fold for morphological examination. After staining with Janus green B for 10 minutes, the mitochondria were observed under a light microscope. For protein analysis, the mitochondrial fraction

was lysed using a mitochondrial lysis buffer to extract mitochondrial proteins. Subsequently, the mitochondrial marker COXIV (cat.#:250135, ZEN-BIO, China, dilution1:1000), and the cytosolic marker GAPDH (cat.#:390035, ZEN-BIO, China, dilution1:1000) were detected by Western blotting in both the mitochondrial and cytosolic fractions, respectively.

Zbp1 siRNA transfection

Transfection was performed using the EndoFectionTM MAX transfection reagent (GeneCopoeia, China). Cells were seeded in 12-well plates, with each well receiving a transfection mixture consisting of 5µL of the transfection reagent and 1µg of siRNA. Following transfection, cells were incubated for 36 hours. The sequences of the siRNA primers are provided in Table S2.

Western blotting

Total proteins were extracted with lysis buffer (KeyGEN Biotech, China) supplemented with 100 mM PMSF and a protease inhibitor cocktail to prevent degradation. Protein concentrations were measured by absorbance at 280 nm. Equal amounts of protein were loaded onto SDS-PAGE gels for electrophoretic separation, followed by transfer onto PVDF membranes (Millipore, USA). Membranes were blocked in 5% bovine serum albumin (BSA) for 1 hour at room temperature, then incubated overnight at 4 °C with primary antibodies against TOMM20 (cat.#:382451, ZEN-BIO, China, dilution1:1000), ATP5a1 (cat.#:R381760, ZEN-BIO, China, dilution1:1000), GAPDH (cat.#: 390035, ZEN-BIO, China, dilution1:1000) TFAM (cat.#:ab307302, Abcam, USA, dilution1:1000), Zbp1 (cat.#:13285-1-AP, Proteintech, China, dilution 1:1000), MLKL (cat.#:66675-1-Ig, Proteintech, China, dilution 1:5000), RIPK3 (cat.#: 68786-2-Ig, Proteintech, China, dilution 1:2000), and p-MLKL (cat.#:37333, CST, USA, dilution 1:1000) and p-RIPK3(cat.#:91702, CST, USA, dilution 1:1000), with antibody dilutions as recommended by the manufacturers. After washing, membranes were treated with horseradish peroxidase (HRP)conjugated goat anti-rabbit IgG(cat.#: SA00001-2, Proteintech, China, dilution 1:2000) for 1 hour at room temperature. Protein bands were visualized using enhanced chemiluminescence reagents (ZEN-BIO, China) and captured by a Bio-Rad imaging system (Bio-Rad, USA). Band intensities were quantified using ImageJ software.

Ethical statement

The research protocol was reviewed and approved by the Institutional Ethics Committee of the Children's Hospital of Chongqing Medical University (Approval ID: CHCMU-IACUC20220804007).

Statistical analysis

All experiments were performed with at least three independent biological replicates. Statistical analyses and graphing were carried out with GraphPad Prism version 9.0. Results are presented as mean \pm standard error of the mean (SEM). Comparisons between groups utilized Student's t-test or one-way ANOVA depending on the data structure. A P value of less than 0.05 was considered statistically significant.

RESULTS

Transcriptomic profiling uncovers enhanced activation of Zbp1-mediated necroptotic pathways following LPS exposure

To investigate the molecular pathways through which LPS induces gene expression alterations and necroptosis in MH-S cells, we conducted an extensive transcriptomic comparison between untreated control samples and LPS-treated cells (n=5 per group). The differential expression analysis, illustrated by a volcano plot (Figure 1A), identified numerous significantly regulated genes. Notably, Zbp1 showed marked upregulation (log_2 fold change = 4.634, P = 0.000139), highlighting its possible involvement in the cellular response to LPS. GO enrichment revealed that the top ten biological processes predominantly involved cytokine-mediated signaling, cellular responses to LPS stimulation, and inflammatory regulation (Figure 1B). Furthermore, KEGG pathway analysis of the 100 most differentially expressed genes indicated significant enrichment in pathways related to cell proliferation and programmed cell death mechanisms (Figure 1C). Hierarchical clustering focusing on necroptosisassociated genes demonstrated coordinated transcriptional modulation, with 14 genes, including Zbp1, showing increased expression, while 9 genes were downregulated (Figure 1D). Together, these results imply a key role for Zbp1 in mediating necroptotic signaling induced by LPS in alveolar macrophages. The protein-protein interaction (PPI) network identified several key proteins, including RIPK3, RIPK1, and MLKL, as potential interacting partners of Zbp1 (Figure 1E). Subsequently, Reactome pathway enrichment analysis revealed a significant association of Zbp1 with the regulation of necroptosis (Figure 1F).

LPS-induced activation of Zbp1-mediated necroptosis in MH-S cells

Cell death via necroptosis was assessed using Calcein/PI staining, lactate dehydrogenase (LDH) release assays, and examination of the Zbp1/RIPK3/MLKL signaling axis. Flow cytometric analysis showed a dose-dependent rise in the percentage of PI-positive MH-S cells after treatment with LPS at concentrations of 0.5 μg/ml and 1 μg/ml (Figure 2A–B). Correspondingly, LDH activity was significantly elevated in the culture media (Figure 2C). To investigate Zbp1 regulation, quantitative PCR and Western blotting were conducted, revealing marked increases in Zbp1 expression at both transcript (Figure 2F) and protein levels (Figure 2D–E) following LPS exposure. Given mitochondria's critical involvement in programmed cell death pathways^[18], we further explored Zbp1's intracellular localization. Immunofluorescence imaging using MitoTracker Red indicated an upsurge in Zbp1 expression with evident mitochondrial colocalization in cells stimulated by LPS (Figures 2G-H). This observation was corroborated by qPCR analysis of isolated mitochondrial fractions, which displayed elevated Zbp1 mRNA upon LPS treatment (Figure 2I). The isolated mitochondria were validated using Janus green B staining and Western blotting, as shown in Figure S1A-B. Moreover, Western blot results demonstrated significant increases in p-RIPK3 and p-MLKL proteins after LPS stimulation (Figure 2J-L). To further validate the role of Zbp1 in LPS-induced necroptosis in MH-S cells, Zbp1 was specifically knocked down using siRNA (knockdown efficiency validated in Figure S2A-C; the siZbp1-1 sequence was selected for subsequent experiments). Calcein/PI staining revealed that Zbp1 knockdown significantly reduced the proportion of dead cells following LPS stimulation (Figure S2D-E). qPCR was performed to assess Zbp1 mRNA levels following knockdown in MH-S cells. The analysis verified the reduction in Zbp1 expression and revealed that the knockdown cells did not respond to LPS challenge (Figure S2F). The protein levels of Zbp1, p-RIPK3, and p-MLKL were assessed by Western blotting. Zbp1 knockdown resulted in decreased expression of p-RIPK3 and p-MLKL following LPS stimulation (Figure S2G-J). Consistent with its role in necroptosis, the death of Zbp1-knockdown cells was significantly reduced upon LPS challenge. In contrast, these cells remained susceptible to death induced by Nigericin

(pyroptosis inducer), Staurosporine (apoptosis inducer), and RSL3 (ferroptosis inducer), as evidenced by a substantial increase in cell death (Figure S2K-L). Collectively, these data substantiate that Zbp1 is a specific mediator of necroptosis, whereas alternative cell death pathways operate independently of Zbp1. Altogether, these findings suggest that LPS induces necroptosis through Zbp1 activation, mitochondrial targeting, and subsequent engagement of necroptotic downstream effectors in MH-S cells.

LPS-induced mitochondrial dysfunction in MH-S cells

To explore how LPS affects mitochondrial function in MH-S cells, we evaluated several indicators, such as mtROS generation, the opening of the MPTP, and $\Delta\Psi$ m. Both confocal microscopy and flow cytometry analyses showed a significant increase in mtROS levels in cells treated with LPS relative to untreated controls (Figure 3A–C). In addition, LPS exposure facilitated the opening of MPTP (Figure 3D–F) and caused a marked reduction in $\Delta\Psi$ m (Figure 3G–I).

Assessment of mitochondrial bioenergetic status further demonstrated a considerable decrease in ATP synthesis following LPS stimulation (Figure 3J). Correspondingly, the expression of essential mitochondrial proteins, such as TOMM20, TFAM, and ATP5a1, was notably diminished after LPS treatment (Figure 3K–N). Together, these findings provide strong evidence that LPS induces substantial mitochondrial dysfunction in MH-S cells.

LPS-induced inflammatory response in MH-S cells

Macrophages exhibit significant plasticity, enabling them to modify their activation states in response to inflammatory signals to support various immune and homeostatic functions^[19, 20]. To investigate the response of MH-S cells to LPS stimulation, we utilized flow cytometry to measure the levels of CD86 and CD206, surface markers indicative of M1 and M2 macrophage subsets, respectively. Concurrently, qPCR was employed to evaluate the expression of key pro-inflammatory cytokines such as IL-1β, TNF-α, and IL-6, thus defining the inflammatory phenotype of the cells. Flow cytometric data revealed a pronounced increase in CD86-positive cells after LPS exposure, suggesting a polarization toward the M1, or classically activated, macrophage phenotype (Figure 4A–D). Meanwhile, qPCR results showed significant elevation in IL-1β and IL-6 mRNA levels following LPS treatment (Figure 4E–G).

Taken together, these findings demonstrate that LPS stimulation enhances inflammatory signaling in MH-S cells and drives their differentiation towards a proinflammatory M1 state, underscoring LPS's role as a key inducer of macrophage activation.

mtROS depletion restores mitochondrial function in MH-S cells

To investigate the role of mtROS in mitochondrial damage, MH-S cells were preincubated with Mito-TEMPO, a specific mitochondrial ROS scavenger, prior to LPS stimulation. Based on preliminary tests, 1 μ g/mL of LPS was chosen for subsequent experiments.

The levels of mtROS, MPTP opening, and $\Delta\Psi m$ were quantitatively evaluated using confocal imaging, flow cytometry, and JC-1 staining assays. Mito-TEMPO pretreatment significantly attenuated the increase in mtROS induced by LPS in MH-S cells (Figure 5A–C). Moreover, it inhibited MPTP opening (Figure 5D–F) and helped maintain $\Delta\Psi m$, which was otherwise reduced after LPS exposure (Figure 5G–I). Intracellular ATP content was notably higher in cells pretreated with Mito-TEMPO compared to those treated solely with LPS (Figure 5J). Additionally, the TFAM protein levels were significantly elevated following Mito-TEMPO treatment relative to the LPS group (Figure 5K–N). Taken together, these findings demonstrate that Mito-TEMPO-mediated clearance of mtROS effectively mitigates LPS-induced mitochondrial dysfunction in MH-S cells.

mtROS depletion mitigates Zbp1-mediated necroptosis in MH-S cells

To delineate the relationship between mitochondrial dysfunction and necroptosis, we investigated whether eliminating mtROS could modulate Zbp1-mediated necroptosis. Flow cytometry demonstrated a significant reduction in PI-positive cell populations in the LPS + MT group compared to cells treated with LPS alone group (Figure 6A-B). Consistently, Mito-TEMPO pretreatment resulted in decreased LDH levels in the culture supernatant (Figure 6C). To rule out potential cytostatic or off-target effects of Mito-TEMPO, we compared the proportion of PI-positive cells by Calcein/PI staining between the untreated control and MT-only treated MH-S cells. The results showed no significant difference in cell death between the two groups (Figure S3A-B). Additionally, Zbp1 expression was markedly suppressed, and its colocalization with mitochondria was attenuated following Mito-TEMPO administration (Figure 6D-E).

Mitochondrial RNA analysis via qPCR further revealed that clearance of mtROS led to a significant downregulation of Zbp1 transcripts within mitochondria of LPS-exposed MH-S cells (Figure 6F).

To further elucidate the mechanistic basis, Western blot assays were performed to assess the expression of necroptosis-associated markers including Zbp1, RIPK3, p-RIPK3, MLKL, and p-MLKL. Mito-TEMPO pretreatment significantly suppressed the protein levels of Zbp1 as well as the p-RIPK3 and p-MLKL compared to LPS treatment alone (Figure 6G-J). Additionally, in MH-S cells, pretreatment with Mito-TEMPO also reduced the mRNA level of Zbp1 (Figure 6K). Collectively, these findings indicate that neutralization of mtROS attenuates Zbp1-dependent necroptotic signaling in MH-S cells.

mtROS depletion attenuates inflammatory responses in MH-S cells

To investigate how reducing mtROS affects macrophage polarization and inflammatory signaling, we conducted flow cytometry to examine the expression of surface markers associated with M1 and M2 phenotypes, and performed qPCR to evaluate cytokine gene expression. This combined strategy was designed to clarify the impact of mitochondrial restoration and inhibition of Zbp1-driven necroptosis on the inflammatory profile.

Flow cytometry revealed that treatment with Mito-TEMPO alongside LPS led to a notable decline in CD86 fluorescence intensity, indicating a suppression of M1-like macrophage activation (Figure 7A-D). Additionally, transcriptional analysis showed lower mRNA levels of the inflammatory cytokines IL-1β and IL-6 in this group (Figure 7E-G). These results collectively suggest that neutralizing mtROS can reduce inflammatory activation in MH-S cells by shifting macrophage polarization away from the M1 phenotype and curbing cytokine expression.

DISCUSSION

In this study, we identified mitochondrial impairment as a key upstream factor contributing to Zbp1-dependent necroptosis in alveolar macrophages during ALI, which intensifies the inflammatory cascade. Notably, the elimination of mtROS was found to restore mitochondrial integrity. Moreover, it suppressed Zbp1-mediated

necroptotic signaling and inhibited the polarization of macrophages toward the M1 pro-inflammatory phenotype, consequently alleviating lung inflammation (Figure 8).

Excess mtROS disrupts oxidative phosphorylation by impairing the electron transport chain and increasing the permeability of the mitochondrial membrane, thereby amplifying mitochondrial dysfunction and promoting inflammation^[21-23]. In our study, mtROS clearance led to the restoration of mitochondrial membrane potential, restriction of MPTP opening, and enhanced ATP production. Concurrently, key proteins involved in mitochondrial integrity displayed partial recovery, indicating that eliminating mtROS mitigates LPS-induced mitochondrial injury. Notably, mtROS scavenging also reduced mitochondrial Zbp1 accumulation and inhibited the downstream phosphorylation of RIPK3 and MLKL, highlighting mtROS as a critical upstream factor in Zbp1-driven necroptosis. In addition, the levels of proinflammatory cytokines associated with the M1 phenotype were significantly diminished, suggesting that mitochondrial dysfunction promotes necroptosis and inflammatory signaling at least in part via mtROS-mediated Zbp1 activation.

Zbp1, initially characterized as a cytosolic sensor of Z-form nucleic acids through its Zα domains, has emerged as a key mediator in cellular stress pathways, including those driven by oxidative stimuli^[24-26]. Our immunofluorescence findings revealed that LPS exposure led to elevated Zbp1 levels not only in the cytoplasm, but also markedly within the nucleus and mitochondria, with notable colocalization in mitochondrial regions. It should be noted that the mitochondrial localization of Zbp1 requires further experimental validation. Studies employing co-immunoprecipitation or other complementary approaches will be crucial to definitively confirm its mitochondrial presence and identify its direct interaction partners.

The downstream signaling cascade is initiated when Zbp1 functions as a scaffold to facilitate the recruitment and activation of RIPK3, which subsequently phosphorylates MLKL, the key effector responsible for executing necroptosis^[27-30]. Prior research has demonstrated that Zbp1 is capable of triggering RIPK3 activation within the nucleus, resulting in MLKL phosphorylation and subsequent disruption of nuclear integrity, leading to cytoplasmic dissemination of nuclear contents^[31, 32]. In alignment with these findings, our ALI animal model revealed that alveolar macrophages exhibited hallmarks of Zbp1-dependent necroptotic activity (refer to Supplementary Materials).

Furthermore, LPS exposure promoted mtROS accumulation alongside elevated levels of Zbp1, p-RIPK3, and p-MLKL, implying a close mechanistic link between oxidative stress and necroptotic signaling. Notably, pharmacological clearance of mtROS significantly reduced the expression of these necroptosis markers, reinforcing the idea that mtROS is a critical upstream signal driving Zbp1-mediated necroptosis in alveolar macrophages. However, although the role of the Zbp1/p-RIPK3 pathway in ALI mice has been preliminarily validated in this study, the effect of Mito-TEMPO on this pathway in vivo requires further investigation. Future studies utilizing Zbp1 knockout mouse models will be necessary to confirm the in vivo function and elucidate the precise mechanisms of the Zbp1/p-RIPK3 pathway.

Overall, this study uncovers a novel perspective on the upstream mechanisms by which mitochondrial impairment and mtROS initiate Zbp1-dependent necroptosis in the context of ALI. Our results underscore the pivotal function of Zbp1 as a molecular integrator linking oxidative stress, mitochondrial damage, necroptotic signaling, and inflammation. These findings also open up several unanswered questions. For example, it remains to be determined whether mtROS-driven Zbp1 activation results from direct oxidative modifications of the protein itself or through stress-induced Z-RNA formation. Furthermore, the functional significance of Zbp1 translocation between mitochondria and the nucleus is still not well understood. Future investigations should explore upstream modulatory pathways—such as mitochondrial DNA leakage, inflammasome dynamics, or activation of stress-responsive kinases—that may influence Zbp1 expression and necroptotic signaling. In addition, exploring pharmacological inhibitors or gene-editing strategies targeting the mtROS-Zbp1 axis may offer promising therapeutic directions for treating ALI and other inflammatory lung disorders.

CONCLUSION

It is known that necroptosis and mitochondrial dysfunction contribute to inflammation, and that LPS can trigger these processes in various contexts. However, it was not clear whether and how LPS-induced mitochondrial damage specifically in alveolar macrophages is coupled to necroptosis to amplify inflammation, and what the precise molecular mechanism entails. Here, we demonstrate that in alveolar macrophages, LPS-induced mtROS acts as an upstream signal to activate Zbp1, leading to

programmed necroptosis. We further show that this macrophage-specific necroptotic

event is a key driver of the inflammatory cascade and tissue injury in our model.

Therefore, our study provides a new, cell-type-specific mechanistic link between

mitochondrial injury and inflammation via necroptosis, refining the understanding of

ALI pathogenesis.

In summary, we demonstrate that mitochondrial dysfunction in alveolar

macrophages—triggered by LPS and mediated through mtROS-dependent Zbp1

activation—acts as a key driver of inflammatory processes in ALI. Our findings

propose that modulation of mitochondrial homeostasis and interference with Zbp1-

mediated necroptosis in macrophages represent viable therapeutic strategies for

dampening inflammation and preventing tissue damage in ALI. This work provides a

mechanistic foundation for the development of targeted interventions and could help

refine current treatment approaches for inflammatory lung injury.

Conflicts of interest: Authors declare no conflicts of interest.

Funding: This study was supported by The National Natural Science Foundation of

China (No. 82570110), Project of Chongqing Medical Scientific Research Project

(Joint Project of Chongqing Health Commission and Science and Technology Bureau)

(2024QNXM026), China Postdoctoral Science Foundation (2022MD713713),

Specially Funded Project of Chongqing Postdoctoral Science Foundation

(2022CQBSHTB1009), Chongqing Municipal Education Natural Science Foundation

of (KJQN202200419), Scientific Natural Science Foundation Chongqing

(CSTB2023NSCQ-MSX0495), and Children's Hospital of Chongqing Medical

University, National Clinical Research Center for Child Health and Disorders

(NCRCCHD-2022-YP-05).

Data availability: The datasets used and/or analyzed during the current study are

available from the corresponding author on reasonable request.

Submitted: July 28, 2025

Accepted: October 26, 2025

Published online: October 29, 2025

17

REFERENCES

- 1. Ma A, Feng Z, Li Y, Wu Q, Xiong H, Dong M, et al. Ferroptosis-related signature and immune infiltration characterization in acute lung injury/acute respiratory distress syndrome. Respir Res 2023; 24(1):154.
- 2. Gautam A, Boyd DF, Nikhar S, Zhang T, Siokas I, Van de Velde LA, et al. Necroptosis blockade prevents lung injury in severe influenza. Nature 2024; 628(8009):835-843.
- 3. Chen Y, Wu X, Jiang Z, Li X. KAE ameliorates LPS-mediated acute lung injury by inhibiting PANoptosis through the intracellular DNA-cGAS-STING axis. Front Pharmacol 2024; 15:1461931.
- 4. Wang X, Zhao H, Lin W, Fan W, Zhuang T, Wang X, et al. Panax notoginseng saponins ameliorate LPS-induced acute lung injury by promoting STAT6-mediated M2-like macrophage polarization. Phytomedicine 2025; 139:156513.
- 5. Hou F, Shi N, Yuan H, Li B, Xiao J, Xiao K, et al. Targeting alveolar macrophages: a promising intervention for pulmonary infection and acute lung injury. Cell Mol Biol Lett 2025; 30(1):69.
- 6. Nguyen TT, Wei S, Nguyen TH, Jo Y, Zhang Y, Park W, et al. Mitochondria-associated programmed cell death as a therapeutic target for age-related disease. Exp Mol Med 2023; 55(8):1595-1619.
- 7. Flores-Romero H, Dadsena S, García-Sáez AJ. Mitochondrial pores at the crossroad between cell death and inflammatory signaling. Mol Cell 2023; 83(6):843-856.
- 8. Pokharel MD, Garcia-Flores A, Marciano D, Franco MC, Fineman JR, Aggarwal S, et al. Mitochondrial network dynamics in pulmonary disease: Bridging the gap between inflammation, oxidative stress, and bioenergetics. Redox Biol 2024; 70:103049.
- 9. Li N, Liu B, Xiong R, Li G, Wang B, Geng Q. HDAC3 deficiency protects against acute lung injury by maintaining epithelial barrier integrity through preserving mitochondrial quality control. Redox Biol 2023; 63:102746.
- 10. Gao Q, Han X, Wang J, Liu X, Wu W. Crosstalk between mitochondrial quality control and novel programmed cell death in pulmonary diseases. Biomed Pharmacother 2025; 189:118335.

- 11. Chen TH, Hsu CC, Chang CP, Huang CC, Wang YJ. Hyperbaric oxygen therapy attenuates carbon monoxide-induced lung injury by restoring mitochondrial dynamics and suppressing Pink1/Parkin-mediated mitophagy. Environ Pollut 2025; 380:126521.
- 12. Zhong WJ, Zhang J, Duan JX, Zhang CY, Ma SC, Li YS, et al. TREM-1 triggers necroptosis of macrophages through mTOR-dependent mitochondrial fission during acute lung injury. J Transl Med 2023; 21(1):179.
- 13. Zhou Y, Huang X, Jin Y, Qiu M, Ambe PC, Basharat Z, et al. The role of mitochondrial damage-associated molecular patterns in acute pancreatitis. Biomed Pharmacother 2024; 175:116690.
- 14. Gonçalves J, Amaral JD, Capela R, Perry MJ, Braga C, Gaspar MM, et al. Necroptosis induced by ruthenium (II) complexes as mitochondrial disruptors. Cell Death Discov 2024; 10(1):261.
- 15. Lee SH, Shin JH, Park MW, Kim J, Chung KS, Na S, et al. Impairment of Mitochondrial ATP Synthesis Induces RIPK3-dependent Necroptosis in Lung Epithelial Cells During Lung Injury by Lung Inflammation. Immune Netw 2022; 22(2):e18.
- 16. Park W, Wei S, Kim BS, Kim B, Bae SJ, Chae YC, et al. Diversity and complexity of cell death: a historical review. Exp Mol Med 2023; 55(8):1573-1594.
- 17. Zheng M, Kanneganti TD. The regulation of the ZBP1-NLRP3 inflammasome and its implications in pyroptosis, apoptosis, and necroptosis (PANoptosis). Immunol Rev 2020; 297(1):26-38.
- 18. Vringer E, Tait SWG. Mitochondria and cell death-associated inflammation. Cell Death Differ 2023; 30(2):304-312.
- 19. Albers GJ, Michalaki C, Ogger PP, Lloyd AF, Causton B, Walker SA, et al. Airway macrophage glycolysis controls lung homeostasis and responses to aeroallergen. Mucosal Immunol 2025; 18(1):121-134.
- 20. Wang L, Oh TG, Magida J, Estepa G, Obayomi SMB, Chong LW, et al. Bromodomain containing 9 (BRD9) regulates macrophage inflammatory responses by potentiating glucocorticoid receptor activity. Proc Natl Acad Sci U S A 2021; 118(35).
- 21. Zhao M, Wang Y, Li L, Liu S, Wang C, Yuan Y, et al. Mitochondrial ROS promote mitochondrial dysfunction and inflammation in ischemic acute kidney injury by disrupting TFAM-mediated mtDNA maintenance. Theranostics 2021; 11(4):1845-1863.

- 22. Mulumba M, Le C, Schelsohn E, Namkung Y, Laporte SA, Febbraio M, et al. Selective Azapeptide CD36 Ligand MPE-298 Regulates oxLDL-LOX-1-Mediated Inflammation and Mitochondrial Oxidative Stress in Macrophages. Cells 2025; 14(5).
- 23. Jung JW, Wang F, Turk A, Park JS, Ma H, Ma Y, et al. Zaluzanin C Alleviates Inflammation and Lipid Accumulation in Kupffer Cells and Hepatocytes by Regulating Mitochondrial ROS. Molecules 2023; 28(22).
- 24. He J, Zhu Y, Tian Z, Liu M, Gao A, Fu W, et al. ZBP1 senses spliceosome stress through Z-RNA:DNA hybrid recognition. Mol Cell 2025; 85(9):1790-1805.e1797.
- 25. Lai K, Wang J, Lin S, Chen Z, Lin G, Ye K, et al. Sensing of mitochondrial DNA by ZBP1 promotes RIPK3-mediated necroptosis and ferroptosis in response to diquat poisoning. Cell Death Differ 2024; 31(5):635-650.
- 26. Cai ZY, Wu P, Liang H, Xie YZ, Zhang BX, He CL, et al. A ZBP1 isoform blocks ZBP1-mediated cell death. Cell Rep 2024; 43(5):114221.
- 27. Koerner L, Wachsmuth L, Kumari S, Schwarzer R, Wagner T, Jiao H, et al. ZBP1 causes inflammation by inducing RIPK3-mediated necroptosis and RIPK1 kinase activity-independent apoptosis. Cell Death Differ 2024; 31(7):938-953.
- 28. Du J, Liu Y, Lan G, Zhou Y, Ni Y, Liao K, et al. PTRF-IL33-ZBP1 signaling mediating macrophage necroptosis contributes to HDM-induced airway inflammation. Cell Death Dis 2023; 14(7):432.
- 29. Mishra S, Jain D, Dey AA, Nagaraja S, Srivastava M, Khatun O, et al. Bat RNA viruses employ viral RHIMs orchestrating species-specific cell death programs linked to Z-RNA sensing and ZBP1-RIPK3 signaling. iScience 2024; 27(12):111444.
- 30. Li S, Zhang Y, Guan Z, Ye M, Li H, You M, et al. SARS-CoV-2 Z-RNA activates the ZBP1-RIPK3 pathway to promote virus-induced inflammatory responses. Cell Res 2023; 33(3):201-214.
- 31. Zhang D, Hao Y, Yang X, Shi X, Zhao D, Chen L, et al. ASFV infection induces macrophage necroptosis and releases proinflammatory cytokine by ZBP1-RIPK3-MLKL necrosome activation. Front Microbiol 2024; 15:1419615.
- 32. Wang WY, Yi WQ, Liu YS, Hu QY, Qian SJ, Liu JT, et al. Z-DNA/RNA Binding Protein 1 Senses Mitochondrial DNA to Induce Receptor-Interacting Protein Kinase-3/Mixed Lineage Kinase Domain-Like-Driven Necroptosis in Developmental Sevoflurane Neurotoxicity. Neuroscience 2022; 507:99-111.
- 33. Wang Y, Liao K, Liu B, Niu C, Zou W, Yang L, et al. GITRL on dendritic cells aggravates house dust mite-induced airway inflammation and airway

hyperresponsiveness by modulating CD4(+) T cell differentiation. Respir Res 2021; 22(1):46.

FIGURES WITH LEGENDS

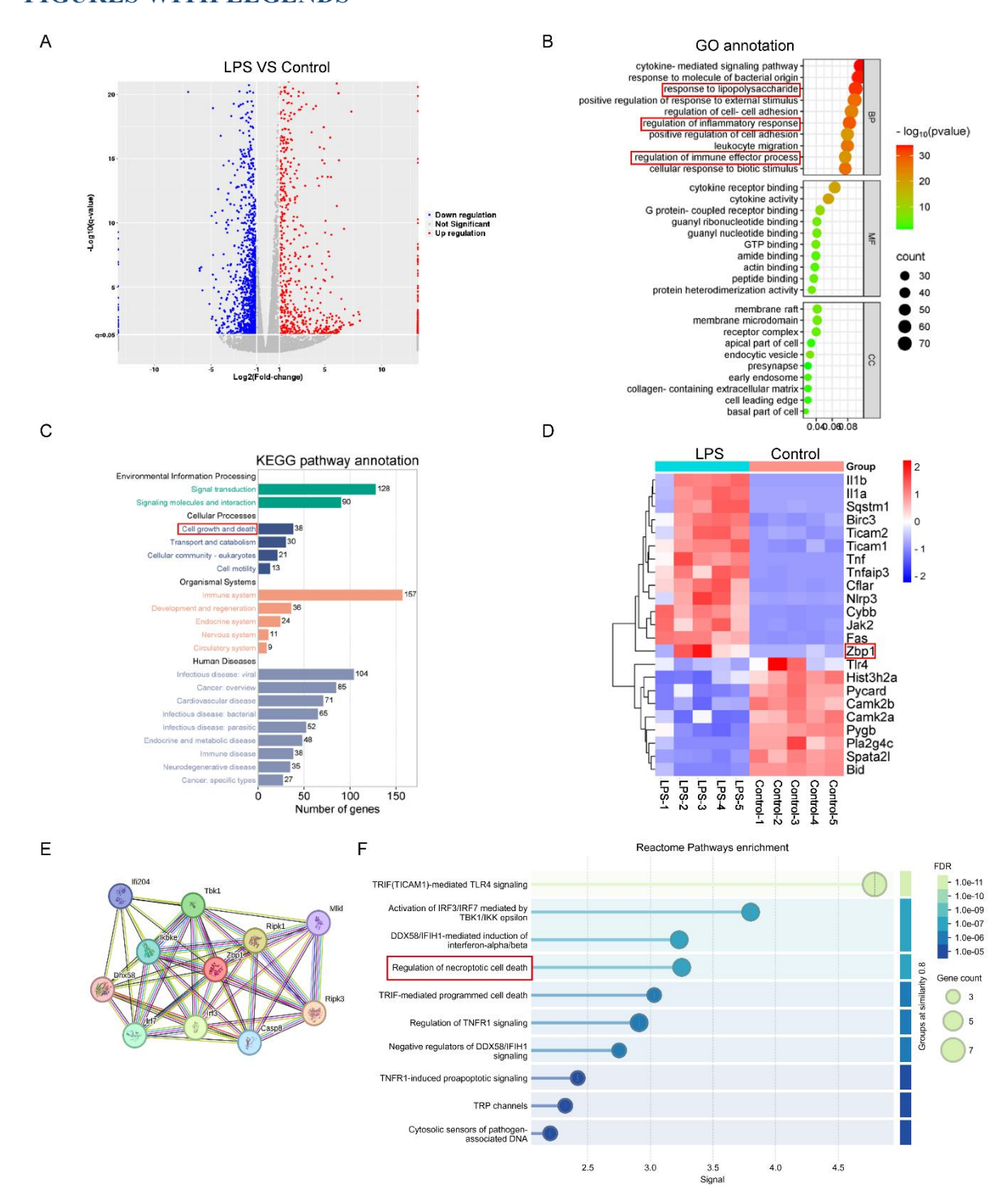


Figure 1. Transcriptomic profiling of LPS-stimulated MH-S cells. (A) Volcano plot illustrating the transcriptomic landscape of differentially expressed genes between LPS-stimulated MH-S cells and untreated control cells. (B) GO enrichment analysis highlighting the top 10 biological processes associated with the most significantly differentially expressed genes. (C) KEGG pathway enrichment analysis of the top 100 differentially expressed genes, emphasizing key molecular pathways

modulated by LPS stimulation. (D) Heatmap visualization of differentially expressed genes specifically related to the necroptosis signaling pathway, showcasing distinct expression patterns. (E) Potential interacting partners of Zbp1 in the PPI network. (F) Reactome pathway enrichment analysis related to the Zbp1 and the interacting partners. Abbreviations: LPS: Lipopolysaccharide; MH-S: Murine alveolar macrophage-like cell line; GO: Gene ontology; KEGG: Kyoto encyclopedia of genes and genomes; PPI: Protein-protein interaction.

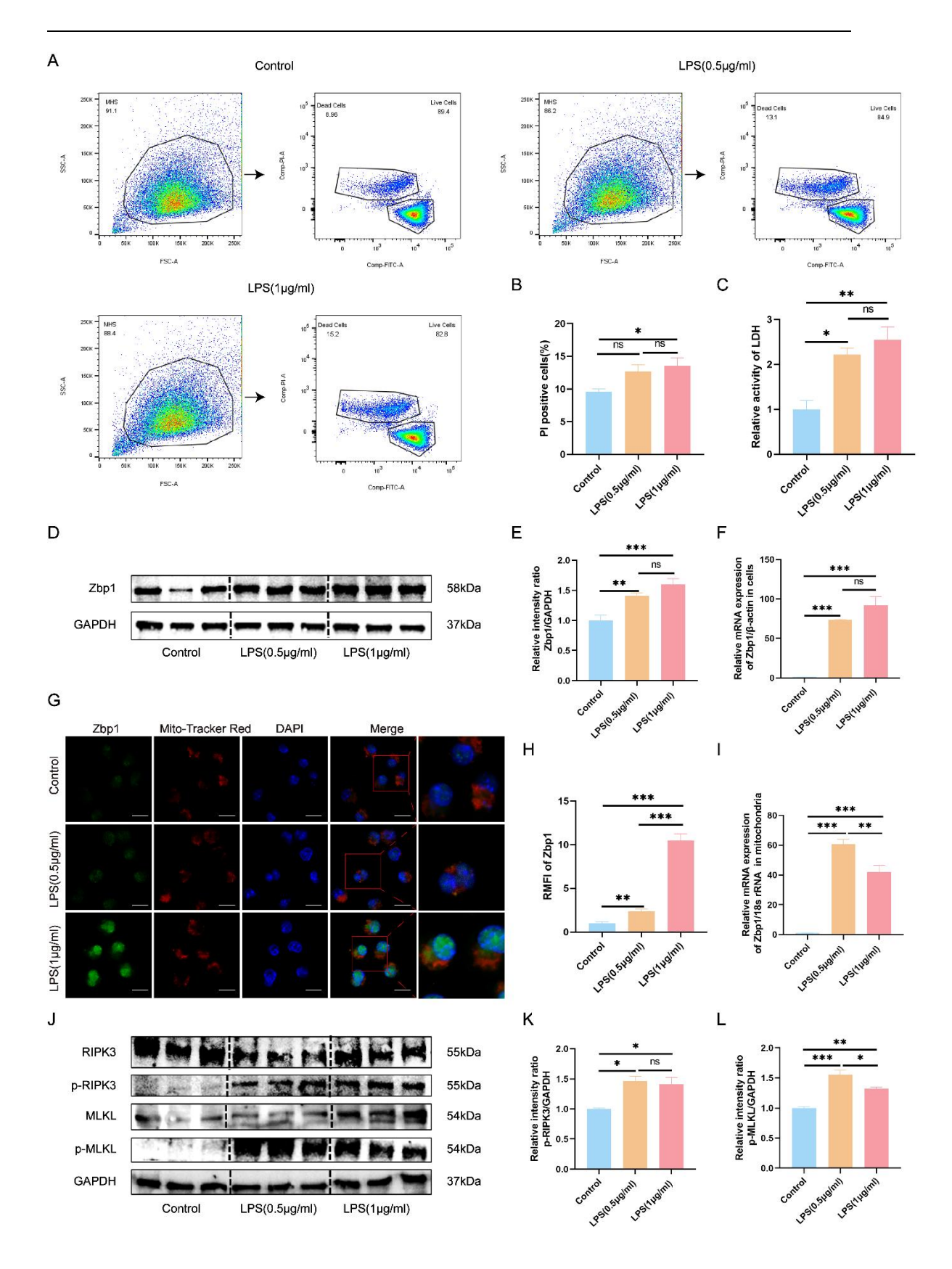


Figure 2. LPS-induced activation of the Zbp1-mediated necroptosis in MH-S cells. (A-B) Flow cytometric analysis using Calcein/PI staining was performed to assess cell viability and necroptosis, and the results were quantitatively analyzed. (C)

Lactate dehydrogenase (LDH) enzymatic activity assays were performed to quantify necroptosis in MH-S cells. (D-E) Western blot analysis was utilized to assess Zbp1 protein expression levels, with GAPDH serving as the loading control. The corresponding densitometric quantifications are presented. (F) Quantitative real-time PCR (qRT-PCR) analysis was performed to evaluate the relative mRNA expression levels of Zbp1 in MH-S cells following stimulation with varying concentrations of LPS. (G-H) Confocal microscopy was used to visualize and quantitatively analyze the colocalization of Zbp1 with mitochondria. Scale bar=25 µm. (I) qRT-PCR analysis was used to assess the relative mRNA levels of Zbp1 localized in the mitochondrial fraction of MH-S cells. (J) Western blot analysis was conducted to evaluate the protein expression levels of RIPK3, p-RIPK3, MLKL, and p-MLKL in MH-S cells, with GAPDH as the loading control. (K-L) Densitometric analysis of the Western blot results for p-RIPK3 and p-MLKL, respectively, is presented. Data are presented as mean \pm SEM, n \geq 3. Normality was assessed using the Shapiro-Wilk test. For one-way ANOVA, Tukey's test was subsequently used for multiple comparisons. Statistical significance was defined as *p < 0.05, **p < 0.01, and ***p < 0.001; ns indicates not significant. Abbreviations: LPS: Lipopolysaccharide; MH-S: Murine alveolar macrophage-like cell line; PI: Propidium iodide; LDH: Lactate dehydrogenase; GAPDH: Glyceraldehyde-3-phosphate dehydrogenase; RIPK3: Receptor-interacting protein kinase 3; p-RIPK3: Phosphorylated receptor-interacting protein kinase 3; MLKL: Mixed lineage kinase domain-like protein; p-MLKL: Phosphorylated mixed lineage kinase domain-like protein; SEM: Standard error of the mean; ANOVA: Analysis of variance.

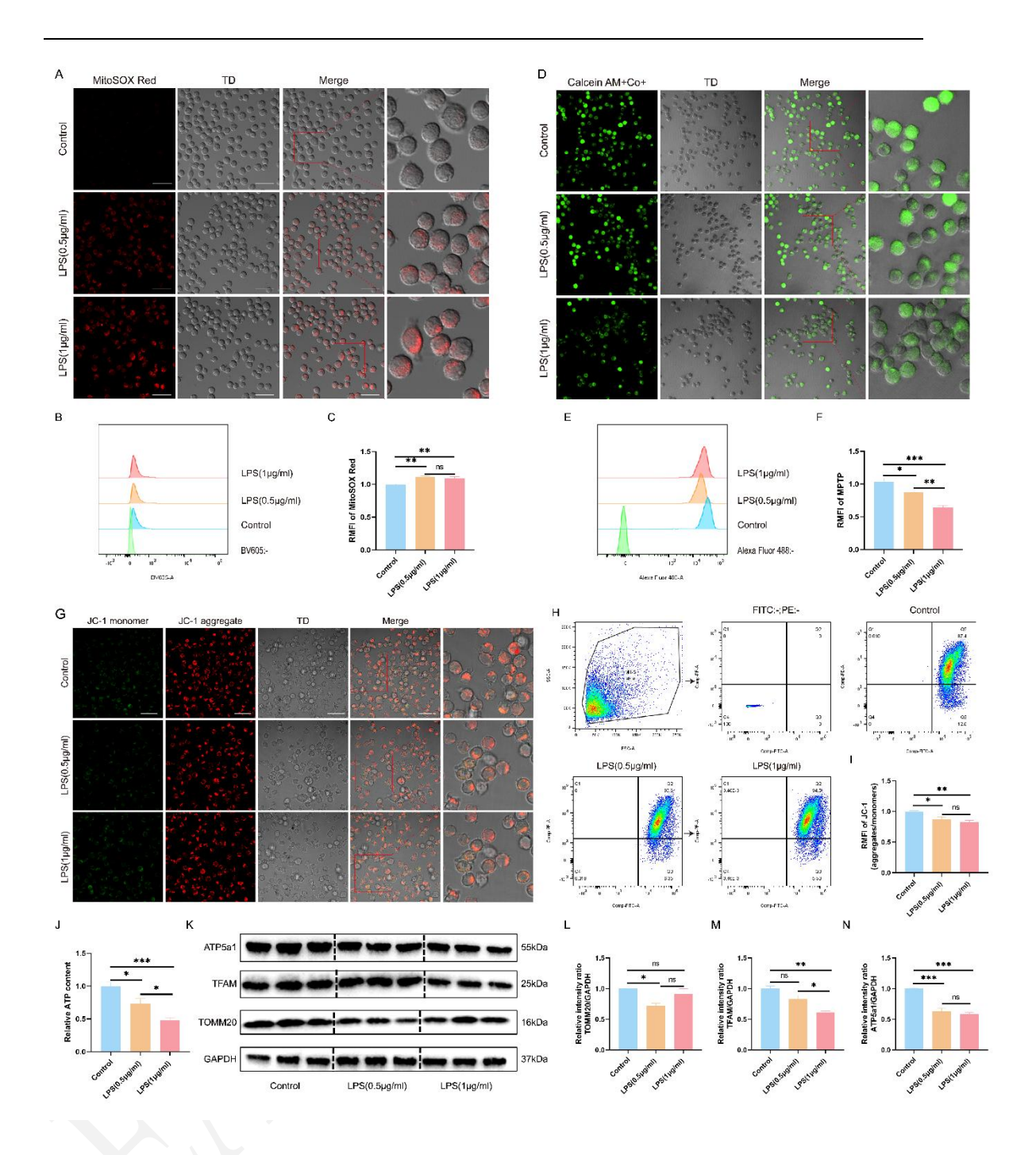


Figure 3. LPS-induced mitochondrial dysfunction in MH-S cells. (A) Confocal microscopy image of MH-S cells stained with MitoSOX Red, highlighting mitochondrial superoxide production. Scale bar = 25 μm. (B-C) Flow cytometry analysis and corresponding quantification of MitoSOX Red fluorescence intensity. (D) Confocal microscopy image of MH-S cells stained with MPTP, reflecting mitochondrial permeability transition pore opening. Scale bar = 25 μm. (E-F) Flow cytometry analysis and corresponding quantification of MPTP fluorescence intensity. (G) Confocal microscopy image of MH-S cells stained with JC-1, demonstrating ΔΨm. Scale bar = 25 μm. (H-I) Flow cytometry analysis and statistical results of JC-1

fluorescence intensity. (J) ATP content measurement in MH-S cells. (K) Western blot analysis of TOMM20, TFAM, and ATP5A1 protein expression in MH-S cells, with GAPDH as the loading control. (L-N) Statistical quantification of TOMM20, TFAM, and ATP5a1 protein expression from western blot data. Data are presented as mean \pm SEM, n \geq 3. Normality was assessed using the Shapiro-Wilk test. For one-way ANOVA, Tukey's test was subsequently used for multiple comparisons. Statistical significance was denoted as *p < 0.05, **p < 0.01, ***p < 0.001, while ns indicated non-significant differences. Abbreviations: LPS: Lipopolysaccharide; MH-S: Murine alveolar macrophage-like cell line; MPTP: Mitochondrial permeability transition pore; $\Delta\Psi$ m: Mitochondrial membrane potential; TOMM20: Translocase of outer mitochondrial membrane 20; TFAM: Mitochondrial transcription factor A; ATP5A1: ATP synthase F1 subunit alpha; GAPDH: Glyceraldehyde-3-phosphate dehydrogenase; SEM: Standard error of the mean; ANOVA: Analysis of variance.

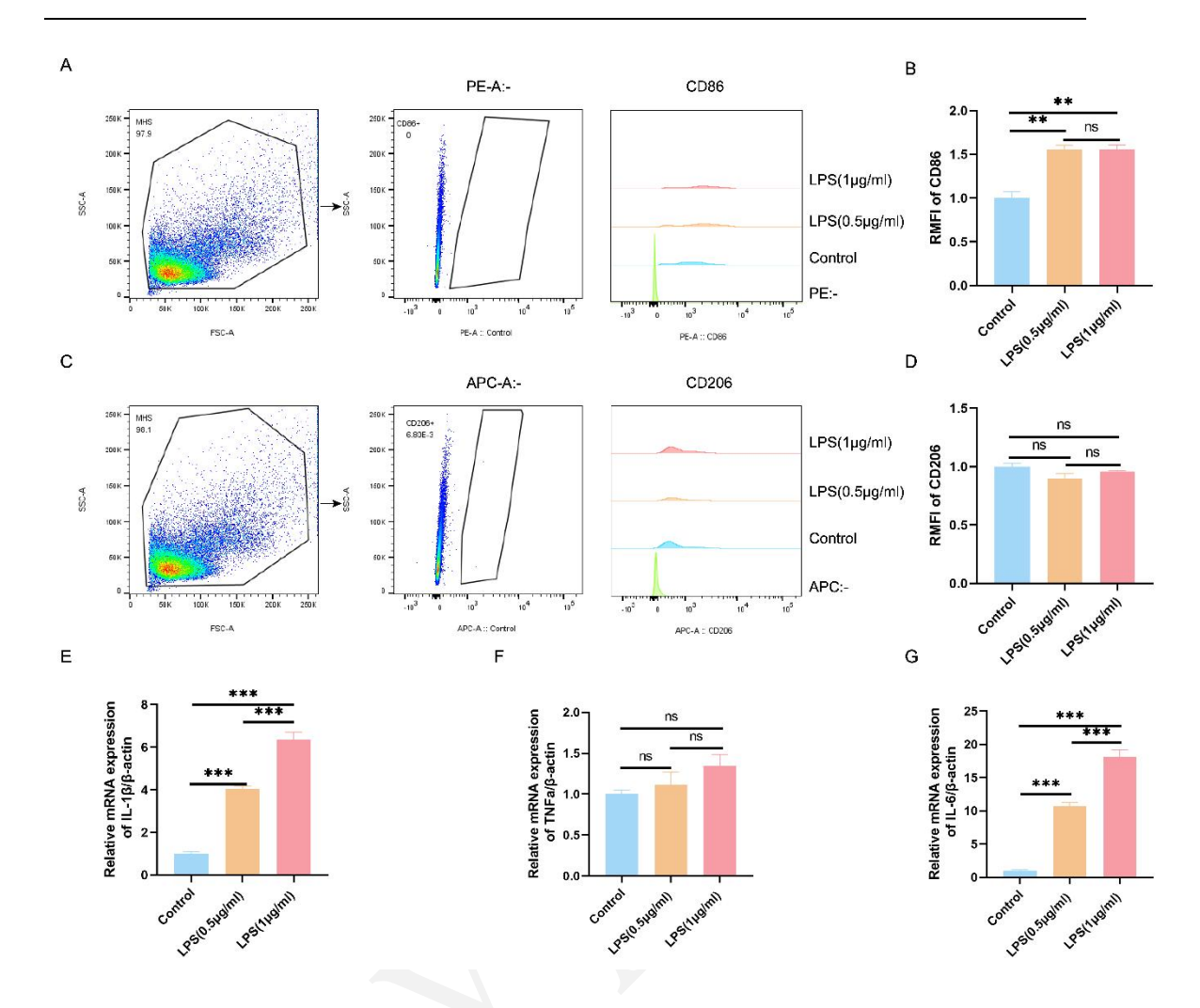


Figure 4. LPS-induced inflammatory response in MH-S cells. (A) Flow cytometric analysis of CD86 expression in MH-S cells following LPS stimulation. (B) Quantitative analysis of the RMFI for CD86 in LPS-stimulated MH-S cells. (C) Flow cytometric analysis of CD206 expression in MH-S cells following LPS stimulation. (D) Quantitative analysis of the RMFI for CD206 in LPS-stimulated MH-S cells. (E-G) qRT-PCR analysis of relative mRNA expression levels of pro-inflammatory cytokines IL-1β, TNF-α, and IL-6 in LPS-stimulated MH-S cells. Data are presented as mean \pm SEM, n \geq 3. Normality was assessed using the Shapiro-Wilk test. For oneway ANOVA, Tukey's test was subsequently used for multiple comparisons. Statistical significance was denoted as **p < 0.01, ***p < 0.001, ns indicated non-significant differences. Abbreviations: LPS: Lipopolysaccharide; MH-S: Murine alveolar macrophage-like cell line; RMFI: Relative mean fluorescence intensity; TNF-α: Tumor necrosis factor alpha; SEM: Standard error of the mean; ANOVA: Analysis of variance.

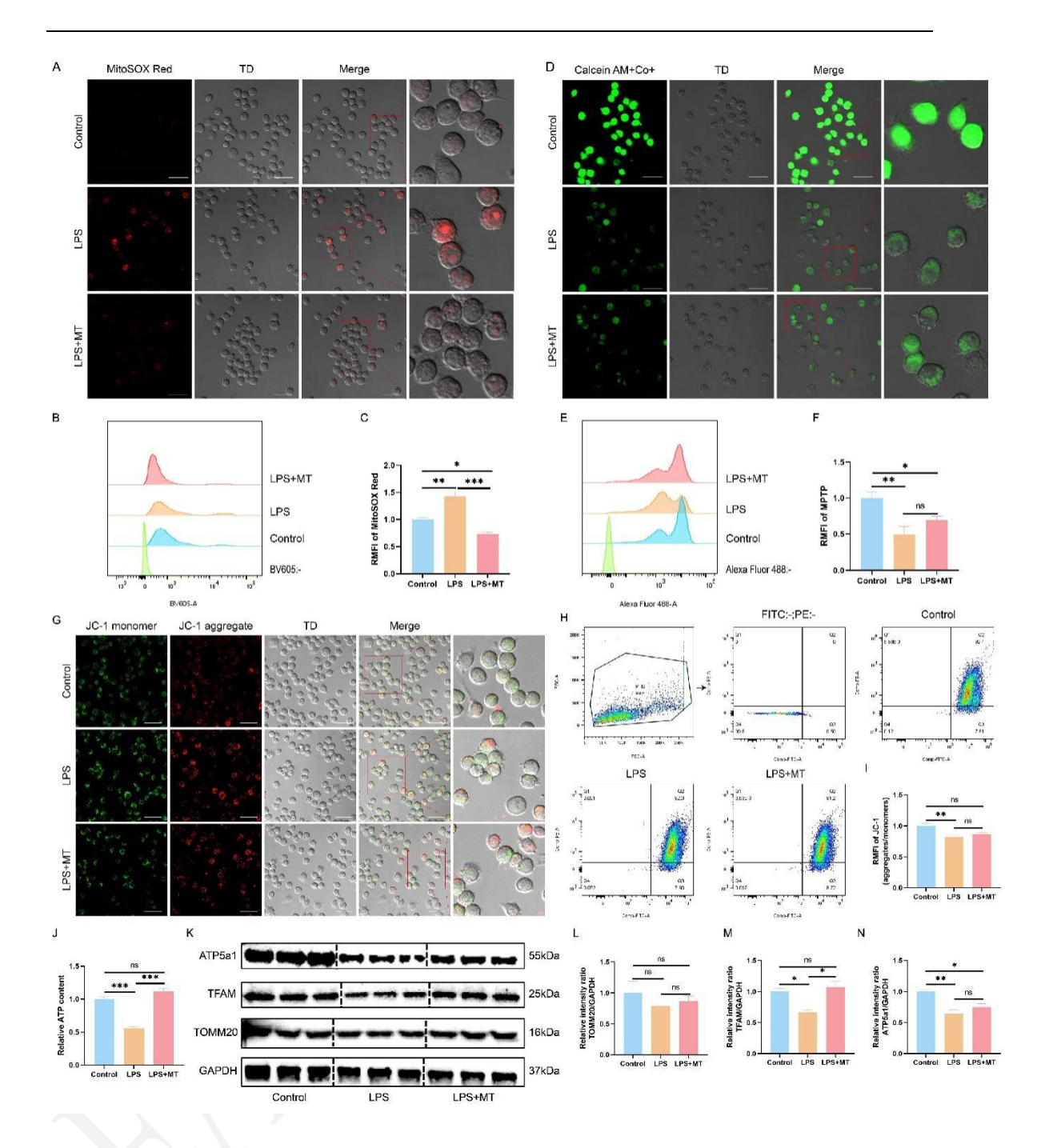


Figure 5. mtROS depletion restores mitochondrial function. (A) Confocal microscopy visualization image of MH-S Cells Stained with MitoSOX Red. Scale bar = 25 μ m. (B-C) Flow cytometric analysis and the statistical result of MitoSOX Red staining in MH-S cells. (D) Confocal microscopy visualization image of MH-S Cells Stained with MPTP. Scale bar = 25 μ m. (E-F) Flow cytometric analysis and the statistical result of MPTP staining in MH-S cells. (G) Confocal microscopy visualization image of MH-S Cells Stained with JC-1. Scale bar = 25 μ m. (H-I) Flow cytometric analysis and the statistical result of JC-1 staining in MH-S cells. (J) ATP content measurement in MH-S cells. (K) Western blot was conducted to quantify the

protein expression levels of TOMM20, TFAM and ATP5a1 in MH-S cells. GAPDH was used as a loading control. (L-N) Statistical results in western blot of TOMM20, TFAM and ATP5a1. Data are presented as mean ± SEM, n ≥3. Normality was assessed using the Shapiro-Wilk test. For one-way ANOVA, Tukey's test was subsequently used for multiple comparisons. Statistical significance was denoted as *p < 0.05, **p < 0.01, ***p < 0.001, while ns indicated non-significant differences. Abbreviations: mtROS: Mitochondrial reactive oxygen species; MH-S: Murine alveolar macrophage-like cell line; MPTP: Mitochondrial permeability transition pore; JC-1: Mitochondrial membrane potential probe; TOMM20: Translocase of outer mitochondrial membrane 20; TFAM: Mitochondrial transcription factor A; ATP5a1: ATP synthase F1 subunit alpha; GAPDH: Glyceraldehyde-3-phosphate dehydrogenase; SEM: Standard error of the mean; ANOVA: Analysis of variance.

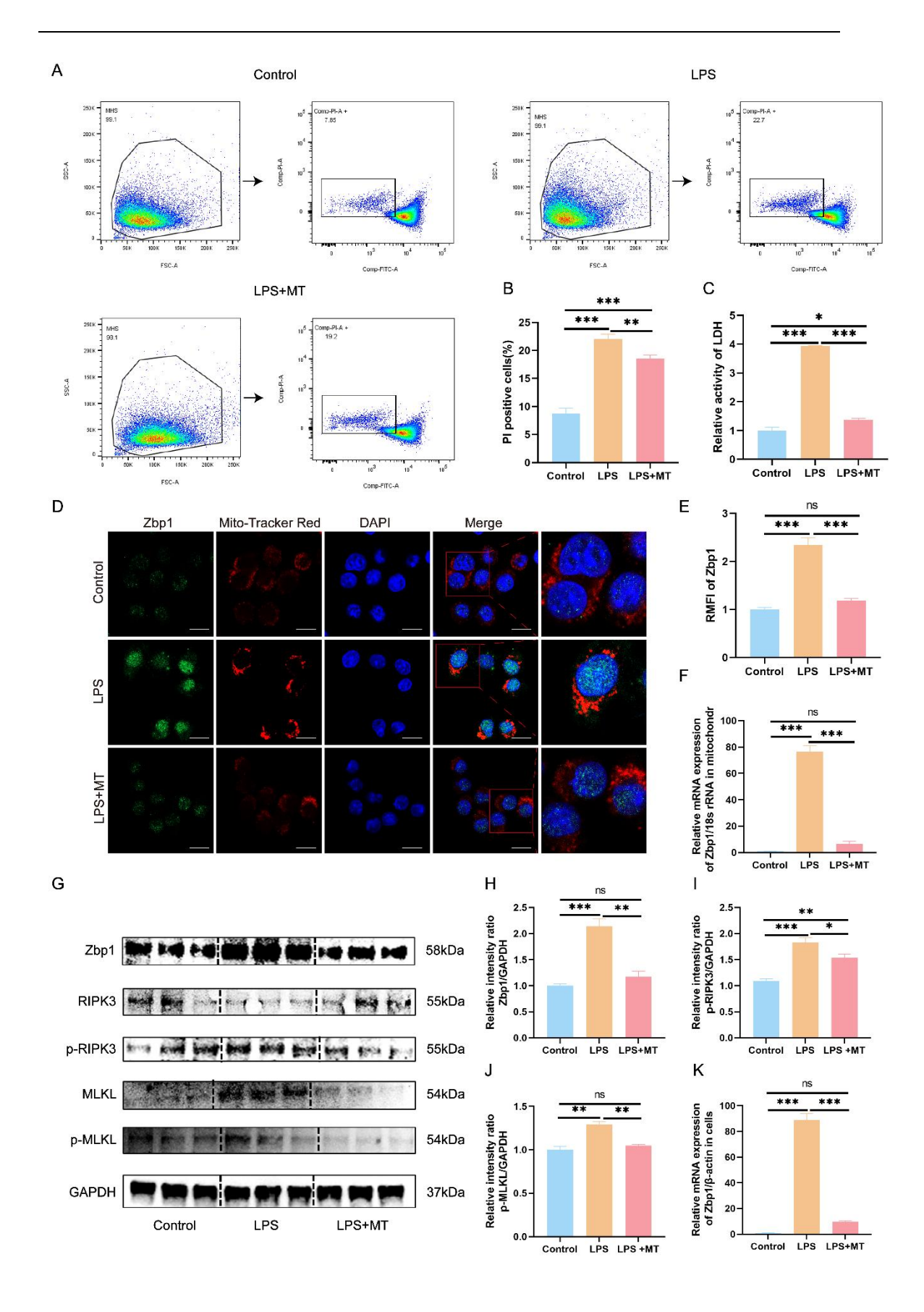


Figure 6. mtROS depletion attenuates Zbp1-mediated necroptosis. (A-B) Flow cytometric analysis and corresponding statistical results of Calcein/PI staining in MH-

S cells. (C) Statistical analysis of LDH enzymatic activity assays in MH-S cells. (D-E) Confocal microscopy visualization of Zbp1 colocalization with mitochondria, with the corresponding statistical representation on the right. Scale bar = 25 µm. (F) qRT-PCR was employed to determine the relative mRNA levels of Zbp1 in mitochondria of MH-S cells. (G) Western blot analysis was utilized to quantify the protein expression levels of Zbp1, RIPK3, p-RIPK3, MLKL, and p-MLKL in MH-S cells. GAPDH served as the internal loading control. (H-J) Statistical analysis of the western blot results for Zbp1, p-RIPK3 and p-MLKL. (K) qRT-PCR was employed to determine the relative mRNA levels of Zbp1 in MH-S cells. Data are presented as mean \pm SEM, $n \ge 3$. Normality was assessed using the Shapiro-Wilk test. For one-way ANOVA, Tukey's test was subsequently used for multiple comparisons. Statistical significance was denoted as *p < 0.05, **p < 0.01, ***p < 0.001, while ns indicated nonsignificant differences. Abbreviations: mtROS: Mitochondrial reactive oxygen species; MH-S: Murine alveolar macrophage-like cell line; PI: Propidium iodide; LDH: Lactate dehydrogenase; RIPK3: Receptor-interacting protein kinase 3; p-RIPK3: Phosphorylated receptor-interacting protein kinase 3; MLKL: Mixed lineage kinase domain-like protein; p-MLKL: Phosphorylated mixed lineage kinase domain-like protein; GAPDH: Glyceraldehyde-3-phosphate dehydrogenase; SEM: Standard error of the mean; ANOVA: Analysis of variance.

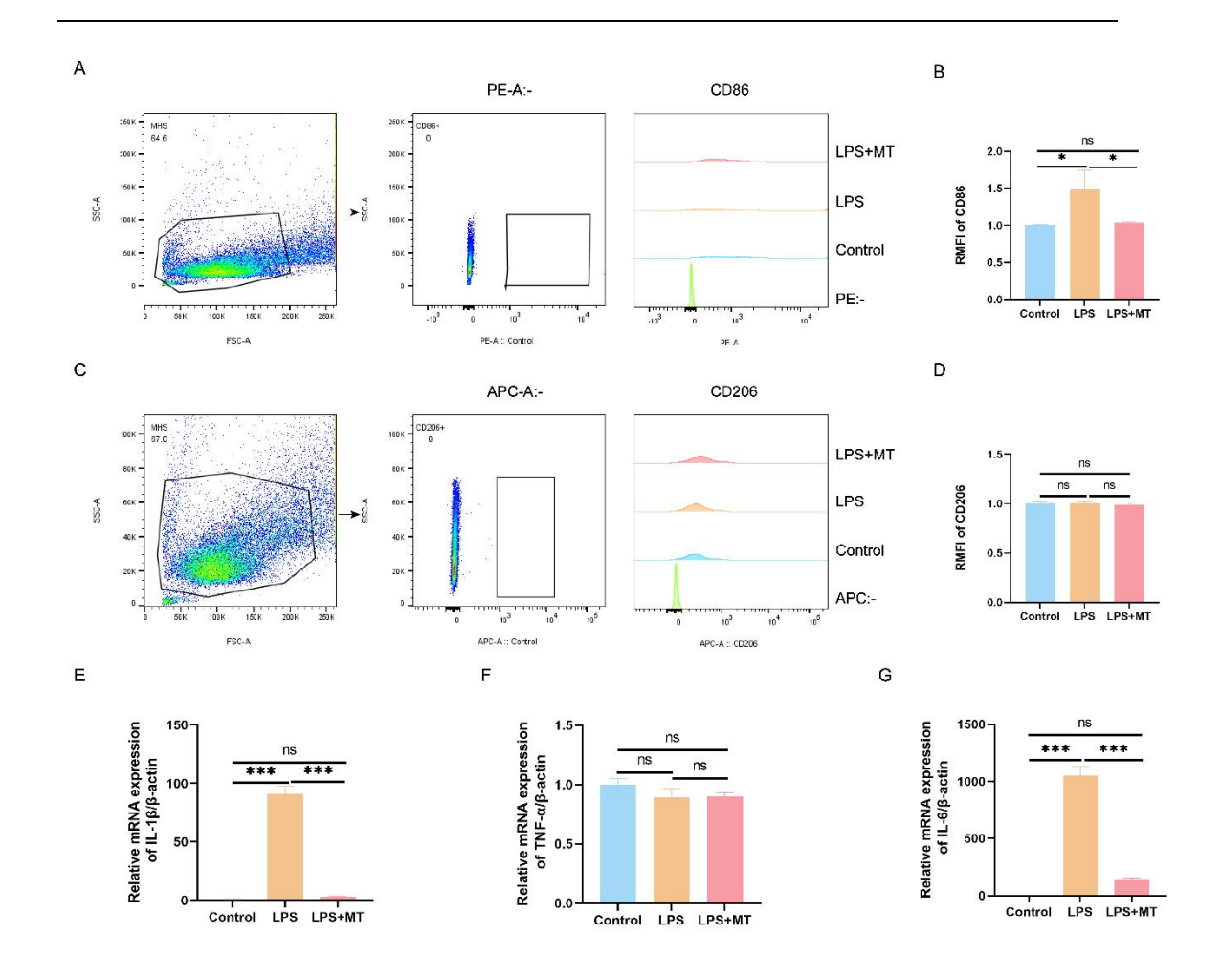


Figure 7. mtROS depletion attenuates inflammatory responses in MH-S cells. (A) Representative flow cytometry plots showing CD86 expression levels in MH-S cells. (B) Quantitative analysis of the RMFI of CD86 in MH-S cells. (C) Representative flow cytometry plots showing CD86 expression levels in MH-S cells. (D) Quantitative analysis of the RMFI of CD206 in MH-S cells. (E-G) qRT-PCR was utilized to measure the relative mRNA expression levels of IL-1β, TNF-α, and IL-6 in MH-S cells. Data are presented as mean \pm SEM, n \geq 3. Normality was assessed using the Shapiro-Wilk test. For one-way ANOVA, Tukey's test was subsequently used for multiple comparisons. Statistical significance was denoted as *p < 0.05, ***p < 0.001, while ns indicated non-significant differences. Abbreviations: mtROS: Mitochondrial reactive oxygen species; MH-S: Murine alveolar macrophage-like cell line; RMFI: Relative mean fluorescence intensity; TNF- α : Tumor necrosis factor alpha; IL-6: Interleukin-6; SEM: Standard error of the mean; ANOVA: Analysis of variance.

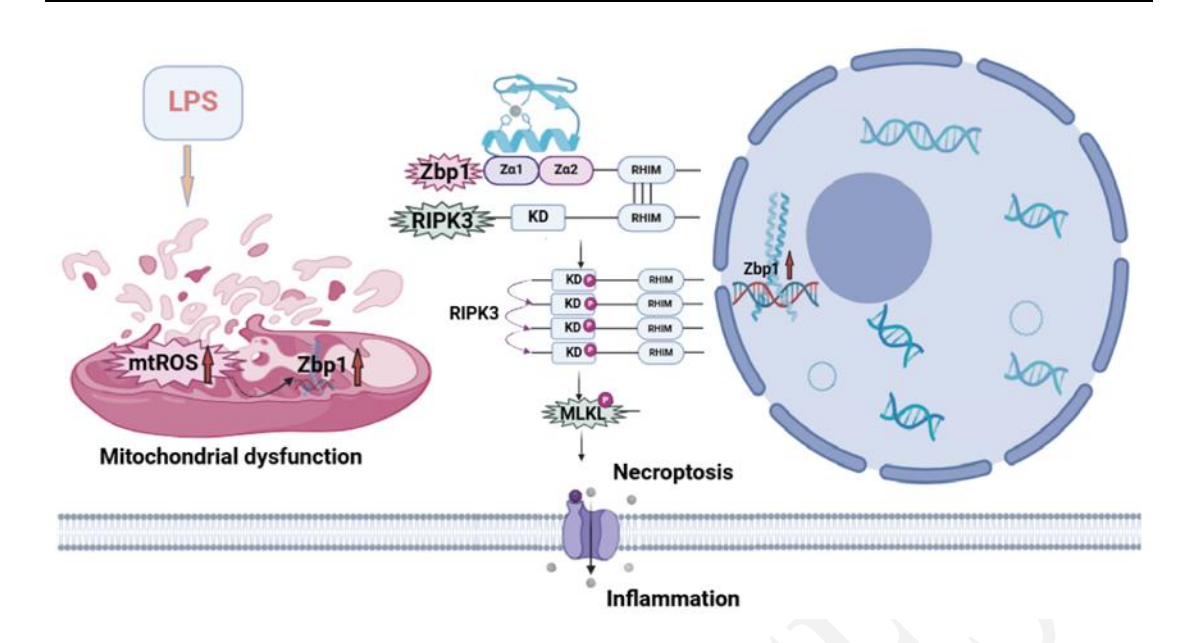


Figure 8. Schematic illustration of Zbp1-mediated necroptosis triggered by mitochondrial dysfunction driving inflammatory responses in alveolar macrophages during acute lung injury. This schematic depicts the pathological mechanism underlying inflammatory responses in alveolar macrophages during ALI. Mitochondrial dysfunction results in the accumulation of ROS, which subsequently activate the Zbp1/RIPK3/MLKL necroptosis pathway. The execution of necroptosis exacerbates inflammation by promoting the release of pro-inflammatory cytokines, thereby amplifying the inflammatory cascade and contributing to ALI progression. Abbreviations: ALI: Acute lung injury; ROS: Reactive oxygen species; RIPK3: Receptor-interacting protein kinase 3; MLKL: Mixed lineage kinase domain-like protein.

SUPPLEMENTAL DATA

Supplemental data are available at the following link:

 $\underline{https://www.bjbms.org/ojs/index.php/bjbms/article/view/13046/4032}$